

# Paramagnon dispersion in $\beta$ -FeSe observed by Fe $L$ -edge RIXS

M. C. Rahn,<sup>1,\*</sup> K. Kummer,<sup>2</sup> N. B. Brookes,<sup>2</sup> A. A. Haghaghird,<sup>1,†</sup> K. Gilmore,<sup>2</sup> and A. T. Boothroyd<sup>1,‡</sup>

<sup>1</sup>*Department of Physics, University of Oxford, Clarendon Laboratory, Oxford, OX1 3PU, United Kingdom*

<sup>2</sup>*European Synchrotron Radiation Facility, BP 220, F-38043 Grenoble Cedex, France*

(Dated: December 15, 2024)

We report an Fe  $L$ -edge resonant inelastic x-ray scattering (RIXS) study of the unusual superconductor  $\beta$ -FeSe. The high energy resolution of this RIXS experiment ( $\approx 55$  meV FWHM) made it possible to resolve low-energy excitations of the Fe  $3d$  manifold. These include a broad peak which shows dispersive trends between 100–200 meV along the  $(\pi, 0)$  and  $(\pi, \pi)$  directions of the one-Fe square reciprocal lattice, and which can be attributed to paramagnon excitations. The multi-band valence state of FeSe is among the most metallic in which such excitations have been discerned by soft x-ray RIXS.

## I. INTRODUCTION

Collective magnetic fluctuations that extend up to hundreds of meV in energy feature prominently in the copper oxide and iron-based families of high temperature superconductors [1, 2]. A detailed understanding of these excitations may reveal important information about the corresponding ground states, such as the strength and character of electronic correlations and itinerancy. Moreover, magnetic fluctuations can lead to unconventional forms of superconductivity, and could play a role in the mechanism of copper oxide and iron-based superconductivity [3–5].

In general, the experimental method of choice to map the spectrum of magnetic fluctuations is inelastic neutron scattering (INS). Modern time-of-flight neutron spectrometers are able to reveal important features of the magnetic spectrum, such as the propagation vector, dispersion, and degree of anisotropy and itinerancy of the magnetism, extending over the entire Brillouin zone with  $\sim$ meV energy resolution [1, 2]. The main drawback of INS is the weakness of the neutron's interaction with the sample, which necessitates sample masses on the order of several grams. For single-crystal studies of materials like  $\beta$ -FeSe, this may require the co-alignment of many hundreds of individual crystallites [6, 7].

By contrast, momentum-resolved x-ray spectroscopic measurements at third generation synchrotrons can be performed on crystals with dimensions below  $100\ \mu\text{m}$ , but face different challenges. The signal from the relevant excitations may be weak, especially if the scattered beam is to be analysed with an extreme energy resolving power ( $E/\Delta E \approx 14,000$  in the present study), and may be complicated by other processes. In the soft x-ray regime, the maximum momentum transfer accessible may not be sufficient to probe the entire Brillouin zone, and the attenuation of the beam adds to the difficulties, requiring ultra-high vacuum (UHV) conditions.

Recent advances in soft x-ray resonant inelastic x-ray scattering (RIXS) instrumentation have significantly improved the

combined energy resolution, and now allow a continuous variation of scattering angle without breaking UHV conditions [8]. In combination with the extreme brilliance of focused undulator beams, the soft-x-ray RIXS technique provides a complementary probe to INS for studies of the low-energy collective dynamics at the heart of correlated electron phenomena [9].

$\beta$ -FeSe (below “FeSe”) remains one of the most puzzling cases among iron-based superconductors (IBSCs) [10, 11]. Structurally, FeSe is the simplest member in the IBSC family, featuring the basic antifluorite layer motif, i.e. square layers of Fe atoms that are tetrahedrally coordinated by a pnictogen or chalcogen, see Fig. 1(a). However, the behaviour of FeSe deviates from the typical behaviour of IBSCs. The pure material enters a superconducting state ( $T_c = 9\text{ K}$ ) without chemical doping, yet  $T_c$  is unusually sensitive to other tuning parameters, rising to  $37\text{ K}$  under pressure [12],  $50\text{ K}$  by intercalation [13], and up to  $100\text{ K}$  in monolayers [14, 15].

Furthermore, whereas typical IBSCs develop superconductivity on suppression of a coexisting antiferromagnetic (AFM) and structurally-distorted nematic phase, in FeSe the nematic phase coexists with superconductivity, albeit on distinct temperature scales, ( $T_c = 9\text{ K}$ )  $\ll$  ( $T_s = 90\text{ K}$ ). AFM order is absent from the nematic phase of FeSe, but strong cooperative paramagnetic spin fluctuations are observed [16, 17]. Very recently, quasiparticle interference studies have revealed that the unusual superconducting gap configuration in FeSe favors pair formation only between  $d_{yz}$  orbitals [18]. In effect, the ground state of FeSe appears to be shaped by competing structural, electronic and magnetic degrees of freedom. The question remains which (or rather, which combination) of the associated fluctuations (lattice, orbital or magnetic) is driving the strange superconducting state in this material [19, 20].

As an advanced technique with the potential to probe both orbital and magnetic correlations, RIXS is particularly promising for disentangling the relevant interactions of this unusually complex ground state. Direct RIXS involves the observation of a net energy transfer after a two-step process in which a core-hole is first created and then recombines with an electron from the valence shell [9]. This contributes to the x-ray scattering amplitude in second order perturbation theory, which implies a strong resonant enhancement when the incident energy coincides with a core-level binding energy [21]. In the context of unconventional superconductivity, soft x-ray RIXS has proven particularly successful in transition metal

\* Present affiliation: Los Alamos National Laboratory, Los Alamos, New Mexico 87545, USA; [rahn@lanl.gov](mailto:rahn@lanl.gov)

† Present affiliation: Karlsruher Institut für Technologie, Institut für Festkörperphysik, Hermann-v.-Helmholtz-Platz 1, D-76344 Eggenstein-Leopoldshafen, Germany

‡ [a.boothroyd@physics.ox.ac.uk](mailto:a.boothroyd@physics.ox.ac.uk)

$L_{2,3}$  edge studies, where  $2p$  core electrons are being excited to the  $d$ -electron valence bands [22].

In the strongly correlated  $3d^9$  magnetic valence state of cuprate superconductors and their parent compounds, RIXS spectra show a sizable response from the dynamic magnetic susceptibility [23], in excellent agreement with neutron inelastic data [24, 25]. In these copper-based materials, superconductivity arises in the vicinity of archetypal localized magnetism, due to one hole confined to a single  $(d_{x^2-y^2})$  orbital. By contrast, for the unconventional superconducting states in iron-based materials, all five  $d$  electronic orbitals are generally considered relevant. Consequently, the valence state of IBSCs is more delocalized and less correlated than in cuprates [26]. The associated magnetism is described as an itinerant phenomenon, arising from the nesting of hole and electron Fermi pockets [27].

This itinerancy has been impeding x-ray spectroscopic studies of electronic correlations in IBSCs, since the dominant fluorescent RIXS response of the Fermi liquid makes it difficult to discern weak excitations of local degrees of freedom [28]. Nevertheless, in principle RIXS promises much more information about the complex multi-band nematic magnetic states of IBSCs than neutron spectroscopy, which simply couples to the dynamic magnetic susceptibility via the magnetic dipole interaction. RIXS should be sensitive to any inter- and intra-orbital electronic dynamics, whether involving spin-flips or not [29]. In this regard, the “local vs itinerant” dichotomy of IBSCs is both promising and problematic. So far, IBSC RIXS has been restricted to the Fe  $K$  edge ( $\approx 7.1$  keV) [30], to large energy transfers at the Fe  $L$  edge [26, 31–33], or to atypically insulating IBSCs [28]. Only the  $L$ -edge RIXS study by Zhou *et al.* (Ref. 34), performed on the  $(\text{Ba},\text{K})\text{Fe}_2\text{As}_2$  system, has succeeded in resolving paramagnon excitations.

Here we report high resolution Fe  $L$ -edge RIXS measurements on FeSe using the new ERIXS end-station of beamline ID32 at the ESRF [8]. With an energy resolution of 55 meV (full-width at half-maximum, FWHM), the present experiment was able to distinguish low-energy dispersive excitations from the (quasi-)elastic peak and fluorescence background. The multi-band valence state of FeSe is among the most metallic systems in which it has been possible to resolve correlated-electron excitations by RIXS. We find that these excitations are qualitatively consistent with cooperative magnetic fluctuations observed in related IBSCs.

## EXPERIMENTAL

High quality single crystals of tetragonal (space group  $P4/nmm$  [35])  $\beta$ -FeSe were synthesized using a  $\text{KCl}-\text{AlCl}_3$  vapor transport technique [36]. The compound crystallizes in the form of platelets with dimensions on the order of  $1\text{ mm}^2$  and  $\approx 200\text{ }\mu\text{m}$  thickness (typical sample mass  $\leq 1\text{ mg}$ ). We characterized these samples by magnetometry and laboratory x-ray diffraction. As discussed in the Supplemental Material [37], these measurements confirmed the high crys-

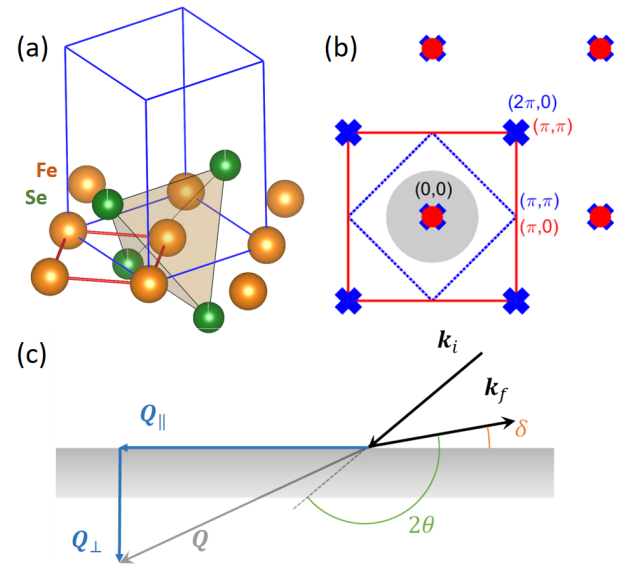


FIG. 1. (color online). (a) Structure of FeSe antifluorite layers with indications of the room temperature tetragonal (blue) unit cell (space group  $P4/nmm$ , lattice parameters  $a = 0.376\text{ nm}$ ,  $c = 0.551\text{ nm}$ ), and the one-Fe (red) unit cell of the square Fe-only lattice ( $a = 0.265\text{ nm}$ ). (b) Two-dimensional view of reciprocal space, showing the tetragonal and one-Fe first Brillouin zones [colors corresponding to panel (a)]. The regime accessible to Fe  $L$ -edge RIXS is shaded gray. (c) Illustration of the scattering geometry of the present experiment. The projection of the momentum transfer onto the  $(\text{HK}0)$  plane,  $\mathbf{Q}_{\parallel}$ , is maximized by choosing a large scattering angle  $2\theta$  and a low grazing angle  $\delta$ . The choice of grazing scattered, rather than grazing incident, geometry minimizes the quasi-elastic background.

talline quality of the samples as well as a sharp onset of the Meissner–Ochsenfeld effect at  $T_c \approx 9\text{ K}$ .

When exposed to air, FeSe crystals tarnish within days. Immediately before the RIXS measurement, a surface layer was therefore stripped from the crystal platelets using an adhesive tape. This revealed a clean, mirror-like surface. The samples were then directly transferred to the UHV system of ID32. Inside the sample chamber, the copper sample carrier is mounted on the goniometer which is connected to the cold finger of a helium flow cryostat via copper braids. Throughout the experiment the sample stage was held at  $\approx 21\text{ K}$ . The beam size at the sample position is  $4 \times 40\text{ }\mu\text{m}^2$  (vert.  $\times$  horz.).

In a compromise for intensity over energy resolution, we configured the spectrometer in its medium-resolution setting, with a combined energy resolution of  $\approx 55\text{ meV}$  FWHM. At the Fe  $L_3$  edge (incident energy  $E_i \approx 707\text{ eV}$ ,  $\lambda \approx 1.75\text{ nm}$ ), we estimate an x-ray penetration on the order of 200 nm into the sample, corresponding to a depth of several hundred unit cells.

A schematic of the present RIXS scattering geometry, which has been widely used for studies of layered superconductors [23, 34, 38], is given in Fig. 1(c). Due to the strongly two-dimensional character of electronic correlations in these materials, a dependence of the spectra on the perpendicular momentum transfer  $Q_{\perp}$  is generally neglected. The same excitation can therefore be probed at different configurations of

scattering and grazing angles ( $2\theta, \delta$ ). To enhance the low-energy excitations and reduce the quasielastic peak, spectra at finite momentum transfer were obtained with a grazing scattered beam. The samples were aligned using the specular (001) reflection, which became accessible by increasing the incident energy to 1.7 keV. Since no other Bragg reflection was accessible as a second reference, the azimuth of the sample was aligned by half-cutting the beam with one edge of the rectangular platelet (which is parallel to a  $\langle 100 \rangle$ -type direction [37]). For all measurements, the incoming beam was linearly (“ $\pi$ ”) polarized in the horizontal scattering plane, and the polarization of the scattered beam was not analyzed.

We refer to reciprocal space coordinates in the conventional “one-Fe” two-dimensional Brillouin zone, see Fig. 1(b). We neglect the orthorhombic distortion and twinning and state coordinates in units of  $1/a$  ( $a = 0.265$  nm), i.e.  $2\pi$  corresponds to one reciprocal lattice unit (r.l.u.). Spectra were measured at a number of scattering angles, with the in-plane momentum transfer  $Q_{\parallel}$  directed either along the  $(1, 0)$  or  $(1, 1)$  direction. As the incident energy is fixed at the Fe  $L_3$  edge, the accessible range of scattering angles ( $50^\circ$ – $150^\circ$ ) imposes kinematic constraints on the scattering process. For FeSe and related IBSCs, the in-plane momentum transfer is limited to approximately  $(0.5, 0)\pi$  and  $(0.35, 0.35)\pi$ , as indicated in Fig. 1(b).

## II. RESULTS

### RIXS response of FeSe

Figure 2(a) shows the total electron yield (TEY) x-ray absorption spectrum (XAS), which is measured as the drain current from the sample surface, over a photon energy range covering the Fe  $L_2$  and  $L_3$  edges. The features observed here, in particular the peak shape and shoulder of the  $L_3$  edge, resemble those observed in other IBSCs, and also of elemental iron [26].

When irradiating the same position on the sample surface for an extended period, we observed a continuous shift of the TEY spectrum towards  $\text{Fe}^{3+}$  character. To confirm that the finite energy excitations of interest in this study are an intrinsic response of bulk FeSe, we measured a number of reference spectra. In these separate experimental sessions (i.e. using different crystals), the samples were periodically translated in the vertical direction, as to avoid irradiating any point on the sample surface for more than five minutes. The consistency of this data with the original measurements indicates that the signal above  $\approx 100$  meV energy transfer is a bulk response, which appears not to be strongly affected by potential surface degradation.

Each RIXS spectrum corresponds to a total data acquisition time of 7–8 hours, at a count rate of on average less than one photon per minute at intensity maxima. To account for variations in resonance strength as a function of incident energy, the data were normalized to the integrated RIXS intensity in the range of 0.5–2.8 eV photon energy loss.

The comparison of raw RIXS spectra shown in Figs. 2(b)

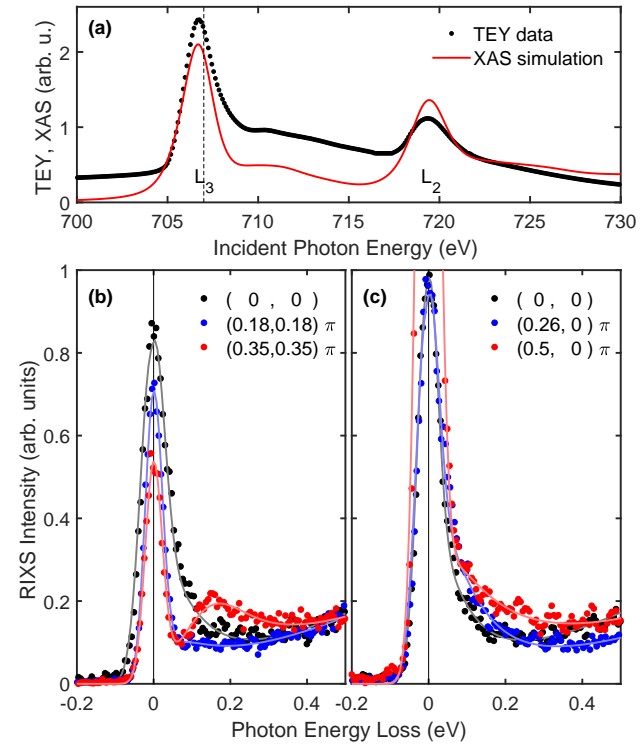


FIG. 2. (color online). (a) Total electron yield (TEY) x-ray absorption spectrum of the Fe  $L_{2,3}$  edges in FeSe, measured as the drain current from the sample surface. The simulated absorption spectrum, calculated in the many-body Bethe-Salpeter equation framework, is shown for comparison. The vertical line indicates the photon energy used in the RIXS experiment. (b)–(c) Comparison of RIXS spectra along the  $(1, 1)$  and  $(1, 0)$  direction. The solid lines are fits to the data (see text for details).

and (c) highlights the low-energy RIXS excitations that form the key interest of this work. The spectra were recorded with varying momentum transfer in the  $(1, 1)$  and  $(1, 0)$  directions, respectively. Close to zero energy transfer, the spectra are dominated by quasielastic scattering. The intensity of this contribution depends on the incident energy, and choice of scattering geometry.

At finite energy transfers, excitations in the continuum of itinerant charge carriers contribute significantly to the measured intensity. In the present spectra, this RIXS fluorescence contributes a sloping background at low energy transfers and forms a broad maximum at  $\approx 1.9$  eV photon energy loss [see Fig. 3(a)]. These characteristics closely resemble measurements of 122 and 1111-type FeAs-based superconductors [26, 34]. In a Fe  $L_3$ -edge RIXS study of the chalcogenide  $\text{Fe}_{1.087}\text{Te}$ , Hancock *et al.* have demonstrated that the slope of the RIXS fluorescence at lower energy losses and its exponential decay above 2 eV are consistent with the Fermi-liquid response to the creation of the core hole [31]. In the present context, these itinerant excitations are not of direct interest.

Additional low energy RIXS excitations are barely resolved at the Brillouin zone center,  $(0, 0)$ , where they appear as a shoulder on the quasielastic peak. However, with increas-

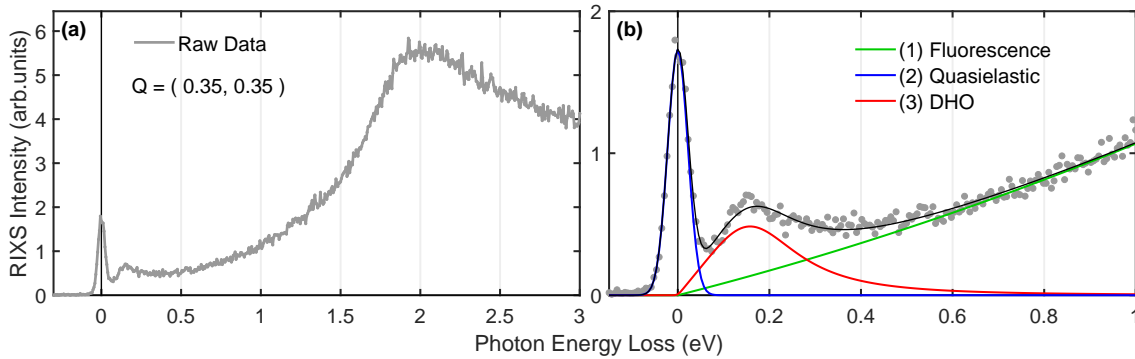


FIG. 3. (color online). (a) Raw Fe  $L_3$  RIXS spectrum of  $\beta$ -FeSe recorded at 21 K, with an in-plane momentum transfer of  $Q = (0.35, 0.35)\pi/a$ . (b) Detailed view of the low-energy region, with lines indicating a least-squares fit of four contributions to the signal.

ing momentum transfer, we observe a systematic increase in these scattering contributions. They are best resolved along the  $(1, 1)$  direction, where they form a distinct peak around 150–200 meV at  $Q = (0.35, 0.35)\pi$ .

### RIXS calculations

To rule out the possibility that the feature appearing around 100–200 meV is due to either electronic orbital excitations or lattice vibrations, we performed first-principles calculations of the electronic contribution to the RIXS spectrum and use a simplified model to estimate the phonon contribution.

The electronic quasiparticle contribution to the RIXS spectrum of FeSe was calculated with the OCEAN code [39–41] by evaluating the Kramers-Heisenberg equation within the framework of the many-body Bethe-Salpeter equation (BSE). The BSE treats excitations within a 2-particle, electron-hole approximation and includes screened direct and bare exchange Coulomb interactions between the electron and hole by summing ladder diagrams. The BSE is well-suited for RIXS calculations as it treats both core-conduction (intermediate-state) and valence-conduction (final-state) excitons on equal footing and does not assume that the final-state exciton is restricted to a localized manifold of  $3d$  states.

We first test the accuracy of the BSE method for FeSe by evaluating the Fe- $L_{2,3}$  X-ray absorption spectrum. The result, shown in Fig. 2(a), is largely in agreement with experiment. The RIXS calculations, shown in Figs. S3(a) and (b) of the Supplemental Material [37], reproduce well the fluorescence contribution, showing a broad peak around 2 eV as observed in the experimental results. Also in accord with experiment, the calculations show essentially no dispersion of the fluorescence contribution. Importantly, the calculation of the quasiparticle contribution goes smoothly to zero at zero energy loss, indicating no appreciable intensity associated with distinct  $d$ -orbital excitations around 100–200 meV.

The BSE calculations are based on a density functional theory electronic structure using the local density approximation (LDA) to the exchange correlation functional. Electronic correlations, beyond those captured by the LDA, can play an im-

portant role in the physical properties of iron-based superconductors, including FeSe. Several quantities, such as effective masses and bandwidths, are not well reproduced by LDA calculations [42]. Computational results are improved by incorporating additional electronic correlations either through the addition of  $GW$  self-energies [43] or by use of dynamical mean field theory (DMFT) [44]. For the XAS calculations presented in 2(a), we have included a  $G_0W_0$  self-energy correction to the LDA electronic structure, which quantitatively improved agreement with the experimental result. We performed the RIXS calculations at the LDA level after finding that inclusion of the  $G_0W_0$  self-energy correction made only small quantitative differences. While a DMFT electronic structure would yield more narrow bandwidths we do not believe this would result in the appearance of pronounced  $d$ -orbital excitations around 100–200 meV in the RIXS calculations.

We provide a rough estimate of the phonon contribution to the RIXS spectrum using a simple model [45] for the coupling of a localized electronic excitation to a local vibrational mode. This model includes as parameters the vibrational frequencies, the coupling strength between the electronic excitations and the phonon, and the RIXS intermediate-state core-hole lifetime. Neutron experiments have shown that vibrational excitations in FeSe are constrained to energies below a sharp cutoff at 40 meV [16, 46]. Electron-energy-loss spectra reported by Zakeri *et al.* reveal dominant phonon modes centered at 20.5, 25.6 and 40 meV [47]. The core-hole lifetime corresponds to that of the Fe  $2p_{3/2}$  level, which is known to be 180 meV [48]. As illustrated in Fig. S3(c) of the Supplemental Material [37], the resulting RIXS spectrum due to excitation of phonons is peaked around 40 meV. This indicates that single-phonon excitations strongly dominate over the higher-order processes, which contribute a tail of scattering intensity towards higher energies [45, 49]. For realistic electron-phonon coupling strengths in FeSe, we can therefore exclude the possibility that the pronounced RIXS excitations above 100 meV are due to lattice excitations. In the present spectra, the effects of phonon scattering are likely limited to an asymmetric broadening of the quasielastic line.

### Phenomenological fit

To illustrate the method used to analyze the anomalous low energy excitations, we display in Fig. 3 the RIXS spectrum recorded at  $Q = (0.35, 0.35)\pi$ , together with our phenomenological model. The fit includes a quadratic polynomial representing the RIXS fluorescence, and a Gaussian lineshape at zero energy transfer to approximate quasielastic scattering.

Subtraction of these features reveals the anomalous intensity shown in Fig. 4. As a simple description of these peaks, we use the dynamical structure factor  $S(Q, E)$  of a damped harmonic oscillator (DHO). This model is frequently used to represent the RIXS response of paramagnon excitations [50]. We adopt the expression by Lamsal *et al.*, which encompasses the case of over-damping [51]:

$$S(Q, E) = A \frac{E}{1 - e^{-\beta E}} \frac{2\gamma E_0}{(E^2 - E_0^2)^2 + (E\gamma)^2}. \quad (1)$$

Here,  $Q$  and  $E$  are the momentum and energy transferred to the sample,  $A(Q)$  is a momentum-dependent scale factor,  $\beta = 1/k_B T$  is the inverse Boltzmann temperature factor, and  $\gamma(Q)$  and  $E_0(Q)$  are the momentum-dependent damping constant and the natural (undamped) energy of the fluctuation. The excitation becomes over-damped (i.e. decays exponentially, without oscillation) if  $E_0 < \gamma/2$ .

Least squares fits of datasets representative for the dispersion along the (1,1) and (1,0) directions of reciprocal space are shown in Fig. 4(a) and (b), respectively. We find that fits of all contributions discussed above generally converge without the need to impose constraints on  $A$ ,  $E_0$  or  $\gamma$ . A complete overview of all fitted data is provided in the Supplemental Material [37].

The variation of the fit parameters thus obtained is presented in Fig. 5. The resonance energy  $E_0$  shows a V-shaped dispersion up to  $\approx 200$  meV, with a  $\approx 100$  meV gap at the Brillouin zone center. We detect no strong systematic variation of the integrated intensities. The fitted values of  $\gamma$  are significantly larger than the experimental energy resolution (55 meV). The DHO lineshape thus appears strongly damped or overdamped throughout the accessible momentum space, which is closely reminiscent of RIXS excitations observed in  $\text{La}_{1.77}\text{Sr}_{0.23}\text{CuO}_4$  [50]. This is evidence for the itinerant nature of the magnetic excitations (see e.g. the neutron spectra of  $\text{SrFe}_2\text{As}_2$ , which also show a significant broadening [52]). The large error bars on some of the points reflect the uncertainties that result from fitting several overlapping scattering contributions.

Our analysis succeeds in describing the data with a minimal number of fitting parameters. We emphasize, however, that the measured signal is small and the background complex, and there may well exist other methods to model the data.

### IV. DISCUSSION

For FeSe, as a paramagnetic metal retaining only limited local degrees of freedom, the RIXS response may include not

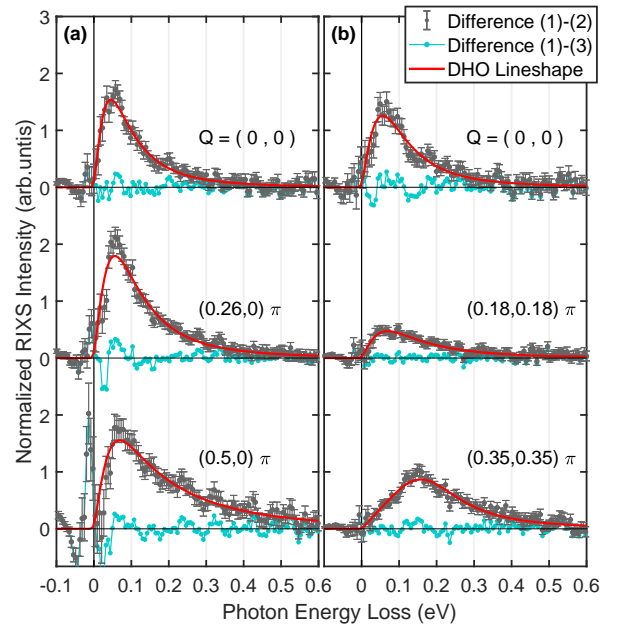


FIG. 4. (color online). Difference signals after subtraction of various fitted components [cf. Fig. 3(b)] from the raw data. Red lines indicate the approximation by a damped harmonic oscillator lineshape. Panels (a) and (b) illustrate representative datasets for momentum transfers along the (1,1) and (1,0) directions, respectively.

only lattice and magnetic excitations, but also non-spin-flip  $d$ - $d$  fluctuations within the five-orbital manifold, as well as Fermi liquid excitations [9, 21]. Our Bethe-Salpeter calculations demonstrate that additional spectral weight peaked in the region of 100–200 meV is unlikely to originate from localized inter-orbital ( $d$ - $d$ ) excitations. Similarly, for reasonable electron-phonon coupling, we are able to rule out dominant phonon scattering in this energy-range. This leaves propagating magnetic fluctuations as the most likely explanation for this signal.

If the response in the present RIXS channels ( $\pi\pi' + \pi\sigma'$ ) is dominated by spin-flip processes, a correspondence with the dynamic magnetic susceptibility measured by INS would be expected. Inelastic neutron studies of FeSe have revealed a spectrum of anisotropic paramagnon excitations [6, 16, 17] steeply dispersing out of  $(\pi, 0)$ , with a band width of about 200 meV, consistent with the RIXS signal.

Due to kinematic constraints, the narrow range of reciprocal space studied by soft RIXS is not directly accessible to inelastic neutron scattering. However, INS can probe equivalent regimes around the  $\Gamma$  points in neighboring Brillouin zones, where the measured paramagnon response should only differ by the reduction in the Fe magnetic form factor. One single crystal INS study has been reported in which Brillouin zone centers were accessed in the energy range of 45–160 meV [17]. In these measurements a suppression of the magnetic scattering was observed at the Brillouin zone center.

Similarly, inelastic neutron studies of more strongly correlated “112” family of IBSCs have found a particularly strong damping of spin fluctuations close to the Brillouin zone cen-

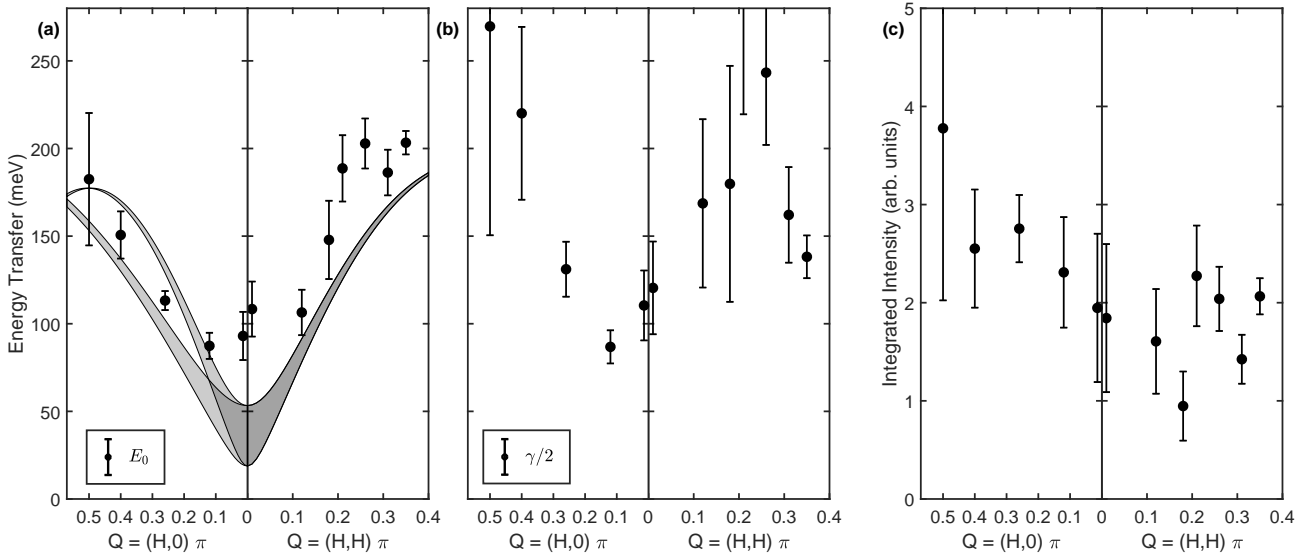


FIG. 5. (color online). Characteristics of low-energy RIXS excitations in FeSe, modeled by a damped harmonic oscillator lineshape, as shown in Fig. 4. Values and uncertainties of (a) natural energies  $E_0$ , and (b) damping parameters  $\gamma$ , obtained from the least squares fits. For comparison, the linear spin wave dispersion inferred from INS measurements on BaFe<sub>2</sub>As<sub>2</sub> [53] is superimposed. The finite width of this curve indicates the range over which the spin wave energies vary for all possible out-of-plane momentum transfers. The splitting along  $(H, 0)$  indicates the variation of the dispersion along the  $a$  and  $b$  axes in a (hypothetical) detwinned sample. (c) Corresponding variation in the integrated intensity of the DHO lineshape. An overview of all fitted datasets is provided in the Supplemental Material [37].

ter [53]. In this case, a comparison is possible to the high-resolution Fe  $L_3$  edge RIXS study of (Ba,K)Fe<sub>2</sub>As<sub>2</sub> reported by Zhou *et al.* [34]. The authors demonstrated a close agreement with the spin-wave model which had been used to model INS spectra, thus providing strong evidence that the RIXS signal is largely due to magnon excitations. By contrast, here we have studied a significantly more itinerant material, with no magnetically-ordered phase available as a reference. As a comparison, in Fig. 5(a) we overlay the linear spin wave model inferred for BaFe<sub>2</sub>As<sub>2</sub> [53] onto the dispersion of the DHO-like lineshape in FeSe.

Several theoretical studies of magnetic fluctuations in FeSe have been reported. Based on density functional calculations, Essunger *et al.* studied the evolution of spin fluctuations as a function of the Se-height parameter  $z_{\text{Se}}$  [54]. While the authors simulated paramagnon spectra only for hypothetical values of  $z_{\text{Se}}$ , a common result appears to be that the paramagnon dispersion is strongly gapped at the Brillouin zone center. Starting from a phenomenological tight-binding model, Kreisel *et al.* have also found paramagnon branches steeply dispersing from a minimum at  $(\pi, 0)$  [55]. However, the characteristics of this dispersion at the Brillouin zone center is unclear, since the calculated dynamic magnetic susceptibility appears to be almost entirely suppressed within  $\approx 0.25$  r.l.u. of the  $\Gamma$  point.

Kaneshita *et al.* have calculated Fe  $L_3$ -edge RIXS spectra based on a five-band Hubbard model of metallic IBSCs [29]. In contrast to cuprates, the authors find that the magnon intensities measured in RIXS are not well separated from  $d$ - $d$  excitations. Instead, the spectra are dominated by orbital excitations that are not associated with a spin-flip. However, the electronic correlations of  $U = 1.2$  eV assumed in these cal-

culations are likely an underestimation in the case of FeSe, where values around  $U \approx 4$  eV are appropriate [44]. Being a description of the itinerant limit in IBSCs, the result by Kaneshita *et al.* may therefore not be applicable to the present data.

## CONCLUSIONS

In conclusion, we have reported a resonant x-ray spectroscopic study at the Fe  $L_3$  edge of the unusual superconductor FeSe, with a combined energy resolution of 55 meV FWHM. The key challenge in this context is the extreme weakness of local excitations in a material where most RIXS spectral weight is due to excitations in the Fermi liquid continuum. We observe significant structure in the low-energy regime, which can likely be associated with magnetic fluctuations.

The excitation energies obtained from fitting a DHO-lineshape to the RIXS spectra reveal a V-shaped dispersion between 100–200 meV, with a large spin-gap at the Brillouin zone center. Since no neutron inelastic study of FeSe is available which has probed the relevant momentum- and energy-transfer regime, and linear spin-wave models proven inadequate [17], the identification of these excitations with the dynamic magnetic susceptibility of FeSe is not straightforward. Nevertheless, our calculations of the RIXS cross section, based on an LDA model of FeSe and knowledge of the principle phonon modes, rule out orbital ( $d$ - $d$ ) or lattice excitations as a possible origin. Instead, the observed dispersion is qualitatively similar to that observed in parent compounds of FeAs-based superconductors.

For correlated itinerant states as in FeSe, the energy

resolution of RIXS is presently limited by the measurable intensity. The realization of this technique's full potential, e.g. including full polarization analysis to distinguish between the orbital character of the excitations, will have to await further advances in synchrotron and beamline instrumentation. Nevertheless, *ab initio* calculations of the RIXS response due to phonons, spin-flip and non-spin-flip orbital excitations to aid a quantitative interpretation of results such as those reported here will be of great interest.

We are grateful to the European Synchrotron Radiation Facility for provision of beamtime at the ID32-ERIXS endstation. This work was supported by the U.K. Engineering and Physical Sciences Research Council (grant no. EP/J017124/1). MCR is grateful for support through the Oxford University Clarendon Fund, the LANL Director's Fund and the Humboldt Foundation. We thank Andrey Geondzhian for assistance with estimating the phonon contribution to the RIXS spectrum.

---

[1] P. Dai, *Rev. Mod. Phys.* **87**, 855 (2015).

[2] D. S. Inosov, *C. R. Physique* **17**, 60 (2016).

[3] D. J. Scalapino, *Rev. Mod. Phys.* **84**, 1383 (2012).

[4] A. Chubukov, *Annu. Rev. Condens. Matter Phys.* **3**, 57 (2012).

[5] M. M. Korshunov, in *Perturbation Theory: Advances in Research and Applications*, edited by Z. Pirogov (Nova Science Publishers Inc, New York, 2018) Chap. 2, pp. 61–138.

[6] S. Shamoto, K. Matsuoka, R. Kajimoto, M. Ishikado, Y. Yamakawa, T. Watashige, S. Kasahara, M. Nakamura, H. Kon-tani, T. Shibauchi, and Y. Matsuda, ArXiv e-prints (2015), [arXiv:1511.04267 \[cond-mat.supr-con\]](https://arxiv.org/abs/1511.04267).

[7] M. Ma, P. Bourges, Y. Sidis, Y. Xu, S. Li, B. Hu, J. Li, F. Wang, and L. Y., *Phys. Rev. X* **7**, 021025 (2017).

[8] N. Brookes, F. Yakhou-Harris, K. Kummer, A. Fondacaro, J. Cezar, D. Betto, E. Velez-Fort, A. Amorese, G. Ghiringhelli, L. Braicovich, R. Barrett, G. Berruyer, F. Cianciosi, L. Eybert, P. Marion, P. van der Linden, and L. Zhang, *Nuclear Instruments and Methods in Physics Research Section A: Accelerators, Spectrometers, Detectors and Associated Equipment* **903**, 175 (2018).

[9] L. J. P. Ament, M. van Veenendaal, T. P. Devereaux, J. P. Hill, and J. van den Brink, *Rev. Mod. Phys.* **83**, 705 (2011).

[10] A. I. Coldea and M. D. Watson, *Annual Review of Condensed Matter Physics* **9**, 125 (2018), <https://doi.org/10.1146/annurev-conmatphys-033117-054137>.

[11] A. E. Böhmer and A. Kreisel, *J. Phys.: Condens. Matter* **30**, 023001 (2018).

[12] S. Medvedev, T. M. McQueen, I. A. Troyan, T. Palasyuk, M. I. Eremets, R. J. Cava, S. Naghavi, F. Casper, V. Ksenofontov, G. Wortmann, and C. Felser, *Nat. Mater.* **8**, 630 (2009).

[13] J. Guo, S. Jin, G. Wang, S. Wang, K. Zhu, T. Zhou, M. He, and X. Chen, *Phys. Rev. B* **82**, 180520(R) (2010).

[14] Q.-Y. Wang, Z. Li, W.-H. Zhang, Z.-C. Zhang, J.-S. Zhang, W. Li, H. Ding, Y.-B. Ou, P. Deng, K. Chang, J. Wen, C.-L. Song, K. He, J.-F. Jia, S.-H. Ji, Y.-Y. Wang, L.-L. Wang, X. Chen, X.-C. Ma, and Q.-K. Xue, *Chin. Phys. Lett.* **29**, 37402 (2012).

[15] J.-F. Ge, Z.-L. Liu, C. Liu, C.-L. Gao, D. Qian, Q.-K. Xue, Y. Liu, and J.-F. Jia, *Nat. Mater.* **14**, 285 (2014).

[16] M. C. Rahn, R. A. Ewings, S. J. Sedlmaier, S. J. Clarke, and A. T. Boothroyd, *Phys. Rev. B* **91**, 180501 (2015).

[17] Q. Wang, Y. Shen, B. Pan, X. Zhang, K. Ikeuchi, K. Iida, A. D. Christianson, H. C. Walker, D. T. Adroja, M. Abdel-Hafiez, X. Chen, D. A. Chareev, A. N. Vasiliev, and J. Zhao, *Nature Communications* **7**, 12182 (2016).

[18] P. O. Sprau, A. Kostin, A. Kreisel, A. E. Böhmer, V. Taufour, P. C. Canfield, S. Mukherjee, P. J. Hirschfeld, B. M. Andersen, and J. C. S. Davis, *Science* **357**, 75 (2017).

[19] A. V. Chubukov, R. M. Fernandes, and J. Schmalian, *Phys. Rev. B* **91**, 201105(R) (2015).

[20] J. Glasbrenner, I. I. Mazin, H. O. Jeschke, P. J. Hirschfeld, R. M. Fernandes, and R. Valentí, *Nature Phys.* **11**, 953 (2015).

[21] W. Schuelke, *Electron Dynamics by Inelastic X-Ray Scattering* (Oxford University Press, 2007).

[22] M. P. M. Dean, *J. Magn. Magn. Mater.* **376**, 3 (2015).

[23] L. J. P. Ament, G. Ghiringhelli, M. M. Sala, L. Braicovich, and J. van den Brink, *Phys. Rev. Lett.* **103**, 117003 (2009).

[24] L. Braicovich, L. J. P. Ament, V. Bisogni, F. Forte, C. Aruta, G. Balestrino, N. B. Brookes, G. M. De Luca, P. G. Medaglia, F. M. Granozio, M. Radovic, M. Salluzzo, J. van den Brink, and G. Ghiringhelli, *Phys. Rev. Lett.* **102**, 167401 (2009).

[25] M. Le Tacon, M. Minola, D. C. Peets, M. Moretti Sala, S. Blanco-Canosa, V. Hinkov, R. Liang, D. A. Bonn, W. N. Hardy, C. T. Lin, T. Schmitt, L. Braicovich, G. Ghiringhelli, and B. Keimer, *Phys. Rev. B* **88**, 020501 (2013).

[26] W. L. Yang, A. P. Sorini, C.-C. Chen, B. Moritz, W.-S. Lee, F. Vernay, P. Olalde-Velasco, J. D. Denlinger, B. Delley, J.-H. Chu, J. G. Analytis, I. R. Fisher, Z. A. Ren, J. Yang, W. Lu, Z. X. Zhao, J. van den Brink, Z. Hussain, Z.-X. Shen, and T. P. Devereaux, *Phys. Rev. B* **80**, 014508 (2009).

[27] A. V. Chubukov, D. V. Efremov, and I. Eremin, *Phys. Rev. B* **78**, 134512 (2008).

[28] H. Gretarsson, T. Nomura, I. Jarrige, A. Lupascu, M. H. Upton, J. Kim, D. Casa, T. Gog, R. H. Yuan, Z. G. Chen, N.-L. Wang, and Y.-J. Kim, *Phys. Rev. B* **91**, 245118 (2015).

[29] E. Kaneshita, K. Tsutsui, and T. Tohyama, *Phys. Rev. B* **84**, 020511 (2011).

[30] I. Jarrige, K. Ishii, M. Yoshida, T. Fukuda, K. Ikeuchi, M. Ishikado, N. Hiraoka, K. Tsuei, H. Kito, A. Iyo, H. Eisaki, and S. Shamoto, *Physica C: Superconductivity and its Applications* **470**, S377 (2010), proceedings of the 9th International Conference on Materials and Mechanisms of Superconductivity.

[31] J. N. Hancock, R. Viennois, D. van der Marel, H. M. Rønnow, M. Guarise, P.-H. Lin, M. Grioni, M. Moretti Sala, G. Ghiringhelli, V. N. Strocov, J. Schlappa, and T. Schmitt, *Phys. Rev. B* **82**, 020513 (2010).

[32] C. L. Chen and C.-L. Dong, in *Superconductors – Materials, Properties and Applications*, edited by A. Gabovich (InTech, Rijeka, 2012) Chap. 2, pp. 21–44.

[33] C. Monney, A. Uldry, K. J. Zhou, A. Krzton-Maziopa, E. Pomjakushina, V. N. Strocov, B. Delley, and T. Schmitt, *Phys. Rev. B* **88**, 165103 (2013).

[34] K.-J. Zhou, Y.-B. Huang, C. Monney, X. Dai, V. N. Strocov, N.-L. Wang, Z.-G. Chen, C. Zhang, P. Dai, L. Patthey, J. van den Brink, H. Ding, and T. Schmitt, *Nat Commun* **4**, 1470 (2013).

[35] S. Margadonna, Y. Takabayashi, M. T. McDonald, K. Kasperkiewicz, Y. Mizuguchi, Y. Takano, A. N. Fitch, E. Suard, and K. Prassides, *Chem. Commun.* **43**, 5607 (2008).

[36] D. Chareev, E. Osadchii, T. Kuzmicheva, J.-Y. Lin, S. Kuzmichev, O. Volkova, and A. Vasiliev, *CrystEngComm* **15**, 1989 (2013).

[37] Supplemental Material attached to this preprint.

[38] L. Braicovich, J. van den Brink, V. Bisogni, M. M. Sala, L. J. P. Ament, N. B. Brookes, G. M. De Luca, M. Salluzzo, T. Schmitt, V. N. Strocov, and G. Ghiringhelli, *Phys. Rev. Lett.* **104**, 077002

(2010).

[39] E. L. Shirley, *Phys. Rev. Lett.* **80**, 794 (1998).

[40] J. Vinson, J. J. Rehr, J. J. Kas, and E. L. Shirley, *Phys. Rev. B* **83**, 115106 (2011).

[41] K. Gilmore, J. Vinson, E. Shirley, D. Prendergast, C. Pemmaraju, J. Kas, F. Vila, and J. Rehr, *Computer Physics Communications* **197**, 109 (2015).

[42] M. Yi, Y. Zhang, Z.-X. Shen, and D. Lu, *npj Quantum Materials* **2**, 57 (2017).

[43] J. M. Tomczak, M. van Schilfgaarde, and G. Kotliar, *Phys. Rev. Lett.* **109**, 237010 (2012).

[44] M. Aichhorn, S. Biermann, T. Miyake, A. Georges, and M. Imada, *Phys. Rev. B* **82**, 064504 (2010).

[45] L. J. P. Ament, M. van Veenendaal, and J. van den Brink, *EPL (Europhysics Letters)* **95**, 27008 (2011).

[46] D. Phelan, J. N. Millican, E. L. Thomas, J. B. Leão, Y. Qiu, and R. Paul, *Phys. Rev. B* **79**, 014519 (2009).

[47] K. Zakeri, T. Engelhardt, T. Wolf, and M. Le Tacon, *Phys. Rev. B* **96**, 094531 (2017).

[48] M. O. Krause and J. H. Oliver, *Journal of Physical and Chemical Reference Data* **8**, 329 (1979), <https://doi.org/10.1063/1.555595>

[49] H. Yavaş, M. van Veenendaal, J. van den Brink, L. J. P. Ament, A. Alatas, B. M. Leu, M.-O. Apostu, N. Wizent, G. Behr, W. Sturhahn, H. Sinn, and E. E. Alp, *Journal of Physics: Condensed Matter* **22**, 485601 (2010).

[50] C. Monney, T. Schmitt, C. E. Matt, J. Mesot, V. N. Strocov, O. J. Lipscombe, S. M. Hayden, and J. Chang, *Phys. Rev. B* **93**, 075103 (2016).

[51] J. Lamsal and W. Montfrooij, *Phys. Rev. B* **93**, 214513 (2016).

[52] R. A. Ewings, T. G. Perring, J. Gillett, S. D. Das, S. E. Sebastian, A. E. Taylor, T. Guidi, and A. T. Boothroyd, *Phys. Rev. B* **83**, 214519 (2011).

[53] L. W. Harriger, H. Q. Luo, M. S. Liu, C. Frost, J. P. Hu, M. R. Norman, and P. Dai, *Phys. Rev. B* **84**, 054544 (2011).

[54] F. Essenerger, P. Buczek, A. Ernst, L. Sandratskii, and E. K. U. Gross, *Phys. Rev. B* **86**, 060412 (2012).

[55] A. Kreisel, S. Mukherjee, P. J. Hirschfeld, and B. M. Andersen, *Phys. Rev. B* **92**, 224515 (2015).

## Supplemental Material:

### Paramagnon dispersion in $\beta$ -FeSe observed by Fe *L*-edge RIXS

M. C. Rahn,<sup>1</sup> K. Kummer,<sup>2</sup> N. B. Brookes,<sup>2</sup> A. A. Haghaghirad,<sup>1</sup> K. Gilmore,<sup>2</sup> and A. T. Boothroyd<sup>1</sup>

<sup>1</sup>*Department of Physics, University of Oxford, Clarendon Laboratory, Oxford, OX1 3PU, United Kingdom*

<sup>2</sup>*European Synchrotron Radiation Facility, BP 220, F-38043 Grenoble Cedex, France*

#### 1. Laboratory single crystal x-ray diffraction

In order to select samples of best crystalline quality, a number of  $\beta$ -FeSe single crystals were characterized by room temperature four-circle Mo  $K_{\alpha}$  x-ray diffraction (Agilent Supernova). The crystals generally grow as rectangular platelets and x-ray diffraction revealed that their edges are parallel to the tetragonal unit cell (space group  $P4/nmm$ , with lattice parameters  $a = 3.77 \text{ \AA}$ ,  $b = 5.52 \text{ \AA}$ ). Figure S1 (b) shows an example of such laboratory x-ray data, where scattered intensity is integrated over a margin perpendicular to the  $(H, K, 0)$  plane of reciprocal space. The in-plane mosaicity of the observed Bragg reflections is smaller than the instrumental resolution ( $\approx 0.6^\circ$ ). Since the material is relatively soft, platelets easily bend, which causes imperfections in the vertical stacking of the atomic planes. Accordingly, crystals with the smallest mosaic spread along the  $(0, 0, L)$  direction were selected for RIXS measurements.

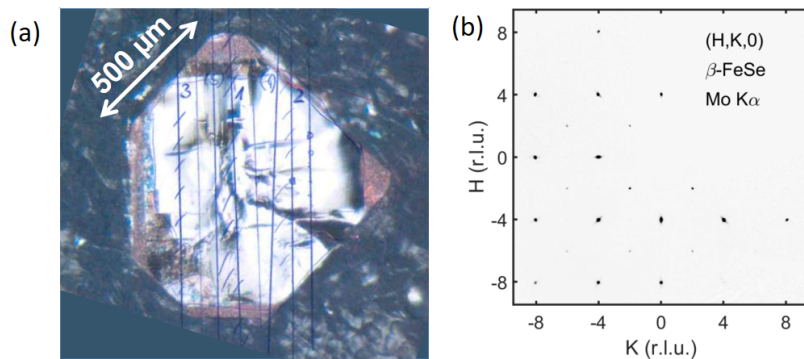


FIG. S1 (color online). (a) Micrograph of a  $\beta$ -FeSe single crystal. The oxidized surface has been stripped from the platelet using adhesive tape. (b)  $(H, K, 0)$  intensity map of reciprocal space, created from Mo  $K_{\alpha}$  four-circle x-ray diffraction data (indexed in space group  $P4/nmm$ ).

## 2. Magnetization

For selected crystallites, we performed magnetization measurements using a superconducting quantum interference device (SQUID, Quantum Design). The zero-field-cooled temperature sweep shown in Fig. S2 illustrates the clean onset of ideal diamagnetism at the superconducting critical temperature  $T_c = 8.9$  K.

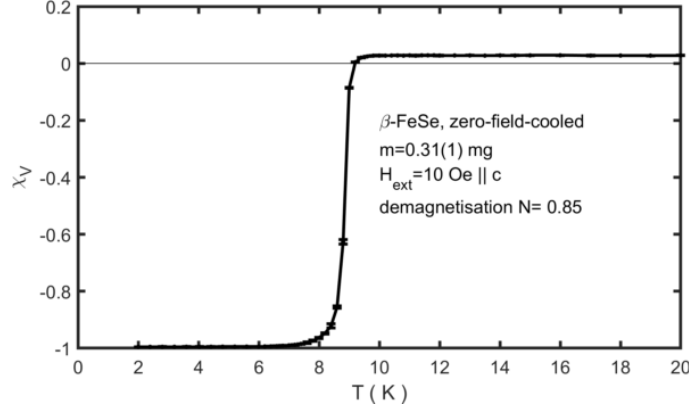


FIG. S2. SQUID magnetometry of a  $0.31(1)$  mg  $\beta$ -FeSe platelet that was used in the RIXS study. The crystal was cooled in zero-field before applying an excitation field of  $10$  Oe along the crystallographic  $c$  axis. The magnetic susceptibility was then measured upon warming, which reveals the superconducting transition at  $T_c = 8.9$  K. The data shown here are normalized under the assumption of a  $100\%$  superconducting volume fraction (demagnetization factor  $N = 0.85$ ).

## 3. Data collection and processing

Due to the thermal drifts of the monochromator, the position of the image on the CCD chip shifts over time. Data were therefore collected in short cycles of around five minutes. To obtain statistics as shown in the main text, the signal was counted for a total of ca.  $7\text{--}8$  cycles for each spectrum.

Several of the spectra were obtained whilst avoiding to irradiate any position on the sample surface for more than five minutes. After each irradiation, the TEY spectra were confirmed to be fully of  $\text{Fe}^{2+}$  character, before slightly translating the sample. Since the vertical size of the beam profile at the sample is very small ( $\approx 4\ \mu\text{m}$ ), this procedure is feasible even for small sample dimensions. Thus we confirmed that the anomalous additional RIXS spectral weight centered around  $150\text{--}300\ \text{meV}$  is a bulk response of FeSe and is not affected by possible surface oxidations processes.

Using the RixsToolBox application, see Ref. [1], all scans comprising one measurement were calibrated and centered with respect to each other by fast Fourier transform and convolution of the spectra. This process did not significantly worsen the effective energy resolution compared to individual datasets, which confirms the reliability of the algorithm. All spectra were obtained in a scattering geometry in which the quasielastic line is observed and a Gaussian peak can be fitted at this position. This serves as a reference of zero energy transfer,  $E = 0$ . The amount of thermal drift over the minimal exposure time required to obtain adequate counting statistics on the quasielastic line is one limiting factor to the energy resolution of the experiment.

#### 4. RIXS fluorescence and phonon calculations

The results of density functional theory (DFT) based Bethe Salpeter equation (BSE) calculations of the fluorescence contribution to the RIXS spectrum are shown in Fig. S3(a)–(b). Calculations assumed the experimental crystal structure. The DFT portion of the spectral calculations were performed with the Quantum-ESPRESSO code [2], which employs pseudopotentials and periodic boundary conditions. We used LDA norm-conserving pseudopotentials with 6 electrons in valence for Se and 16 electrons in valence for Fe. Convergence required a planewave basis energy cutoff of 120 Ry for the wavefunctions and 480 Ry for the charge density. The ground-state charge density was converged with a  $7 \times 7 \times 5$   $k$ -point sampling while  $9 \times 9 \times 7$   $k$ -points were used for the BSE final states. Numerical, full frequency calculation of the  $G_0W_0$  self energy was performed with the Abinit code [3–5].

To estimate the phonon contribution to the RIXS spectra we evaluated a simple model for the coupling of local electronic levels to local vibrational modes [6]. We considered two electronic levels coupled to two vibrational modes of energies 25 meV and 40 meV. The Fe  $2p_{3/2}$  core-hole lifetime was set to the known value of 180 meV HWHM linewidth [7]. For fairly strong values of the coupling constants  $g = (M/\omega_{ph})^2 = 5$  ( $\omega_{ph}$  is the phonon frequency and  $M$  the electron-phonon coupling energy), we find that the phonon RIXS contribution peaks around 40 meV with a rapidly decaying tail to higher energy as shown in Fig. S3(c). Significantly increasing the coupling constants does not shift the peak position, but only causes the high energy tail to decay somewhat more gradually. That the phonon contribution peaks at the first harmonic is a largely inescapable consequence of the relatively short core-hole lifetime of the Fe  $2p_{3/2}$  level and it appears highly unlikely the experimental intensity around 150 meV (equivalent to a third or fourth phonon harmonic) would be vibrational in origin.

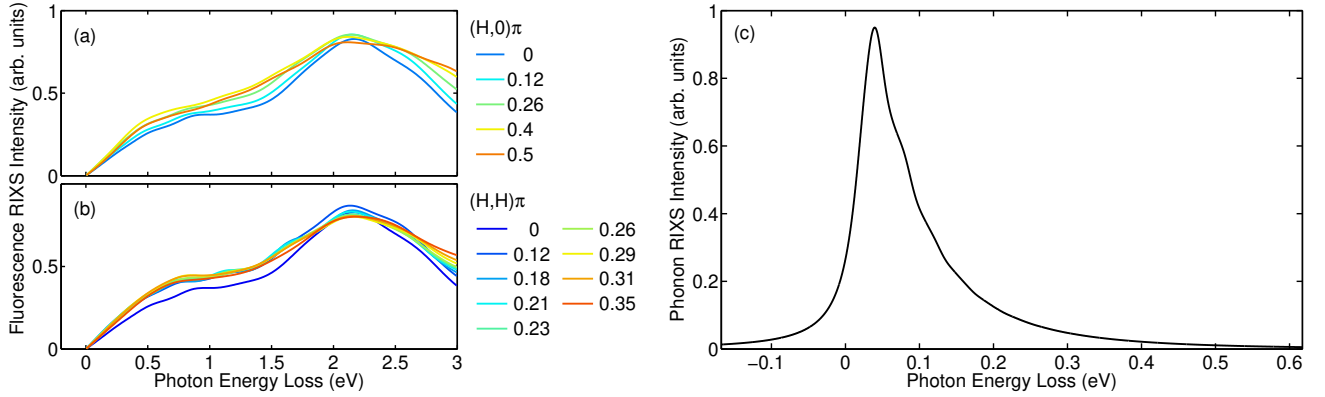


FIG. S3. (a) Electronic quasiparticle contribution to the RIXS spectrum of FeSe, obtained through evaluation of the Kramers-Heisenberg equation within the framework of the many-body Bethe-Salpeter equation. (b) Calculated RIXS phonon spectrum of FeSe, assuming a core-hole lifetime broadening of 180 meV and principle phonon modes at 20.5, 25.5 and 40 meV, as observed in the Raman study by Zakeri *et al.* [8].

## 5. Summary of RIXS spectra

All RIXS spectra used to construct the dispersion shown in Fig. 5 of the manuscript are summarized in Figs. S4 and S5 for the (1,0) and (1,1) directions of reciprocal space, respectively. Subpanels labeled (b) and (c) indicate phenomenological fits of the contributions discussed in the main text, in analogy to Fig. 3 therein.

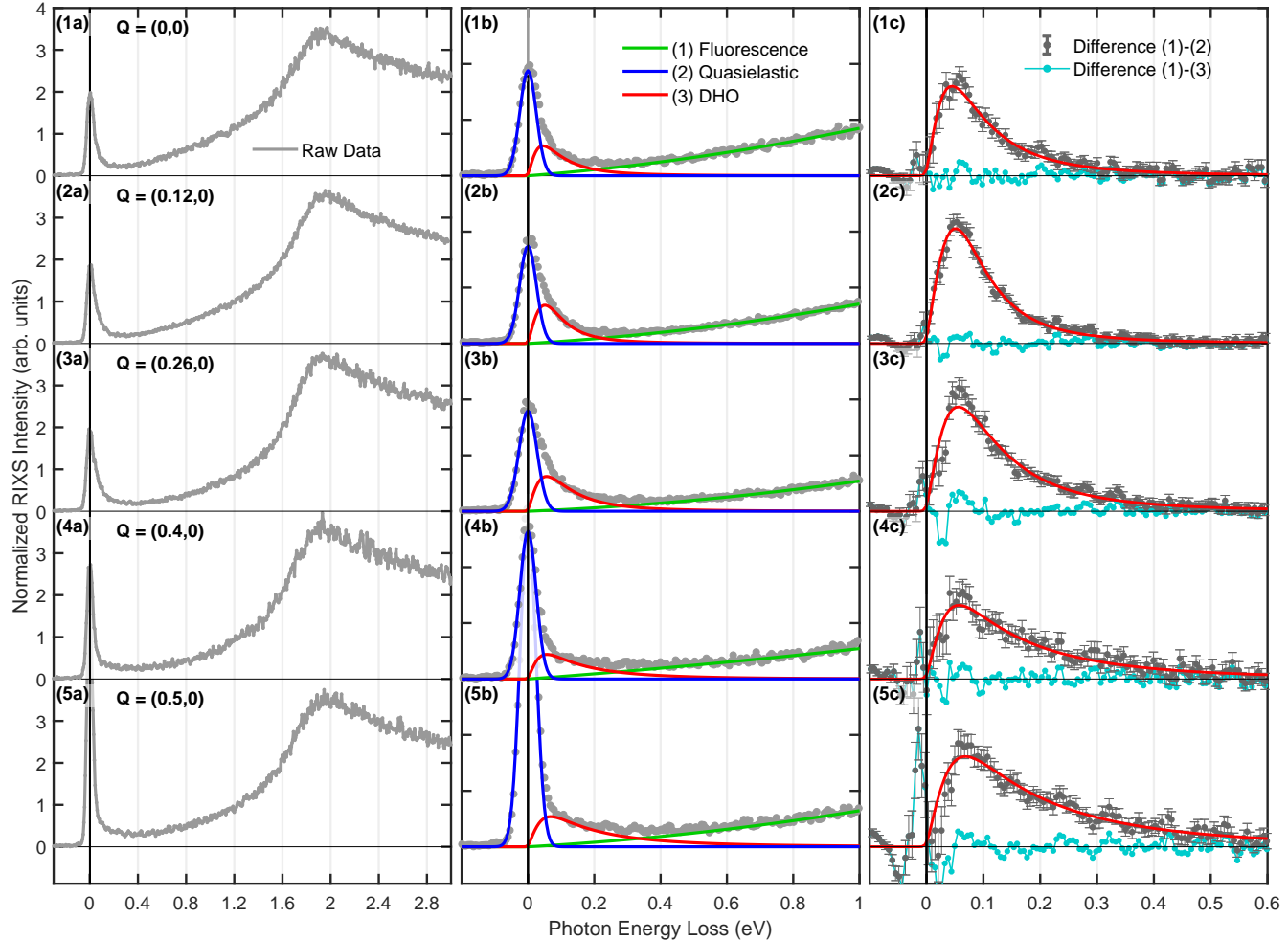


FIG. S4. Fe  $L_3$  RIXS spectra of  $\beta$ -FeSe recorded at 21 K, with an in-plane momentum transfer along the (1,0) direction of reciprocal space. (1a)–(5a) Raw data, dominated by quasielastic scattering and a strong fluorescence contribution. (1b)–(5b) Detailed views of the low-energy region, with curves indicating a fit of three contributions to the signal. (1c)–(5c) Difference signals after subtraction of the quasielastic line and fluorescence contribution (grey errorbars). Residual after additional subtraction of the DHO lineshape (cyan markers).

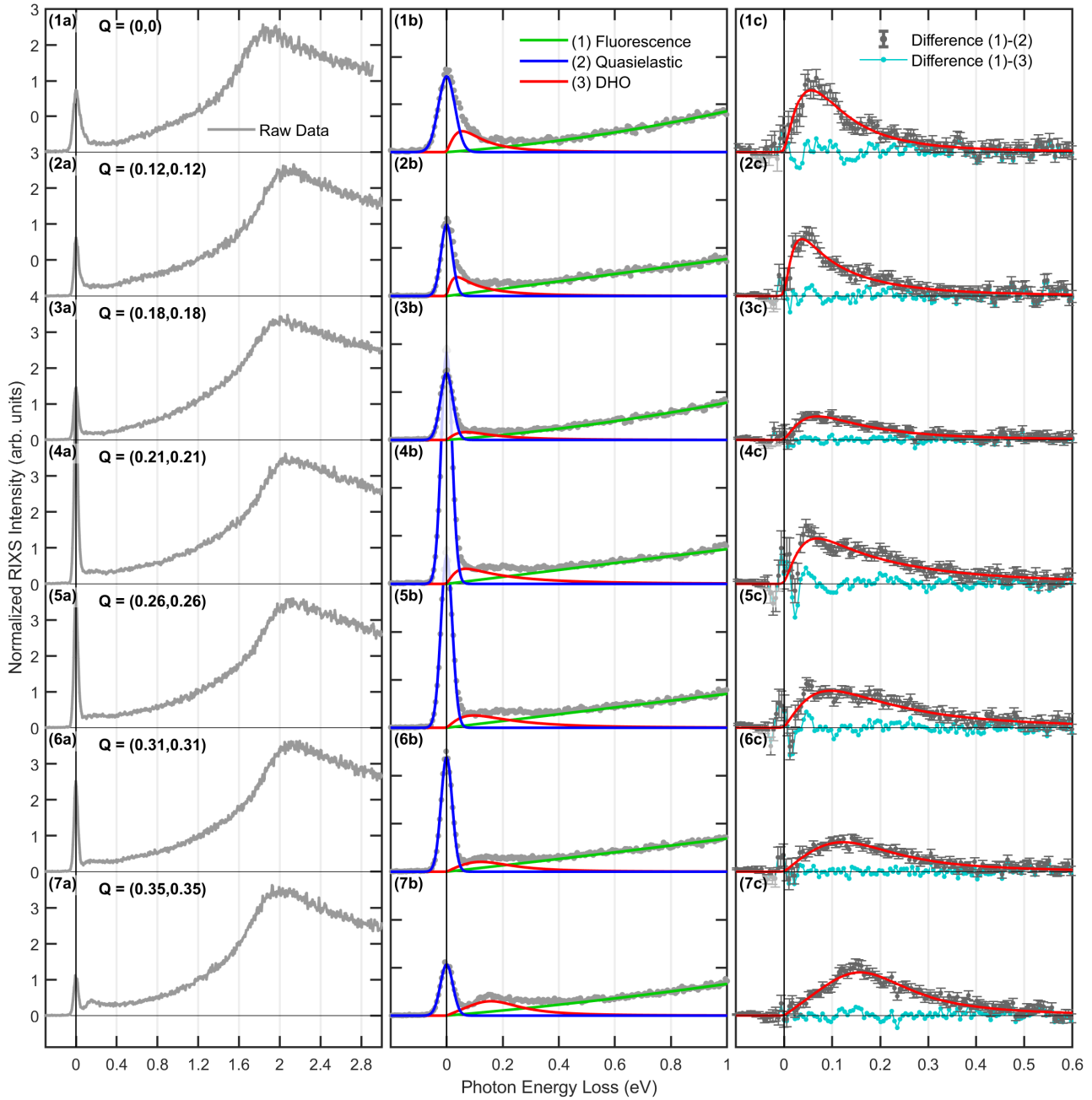


FIG. S5. Fe  $L_3$  RIXS spectra of FeSe recorded at 21 K, with an in-plane momentum transfer along the (1, 1) direction of reciprocal space. The data are presented in analogy to Fig. S4.

---

[1] K. Kummer, A. Tamborrino, A. Amorese, M. Minola, L. Braicovich, N. B. Brookes, and G. Ghiringhelli, *Journal of Synchrotron Radiation* **24**, 531 (2017).

[2] P. Giannozzi, S. Baroni, N. Bonini, M. Calandra, R. Car, C. Cavazzoni, D. Ceresoli, G. L. Chiarotti, M. Cococcioni, I. Dabo, A. D. Corso, S. de Gironcoli, S. Fabris, G. Fratesi, R. Gebauer, U. Gerstmann, C. Gougoussis, A. Kokalj, M. Lazzeri, L. Martin-Samos, N. Marzari, F. Mauri, R. Mazzarello, S. Paolini, A. Pasquarello, L. Paulatto, C. Sbraccia, S. Scandolo, G. Sclauzero, A. P. Seitsonen, A. Smogunov, P. Umari, and R. M. Wentzcovitch, *Journal of Physics: Condensed Matter* **21**, 395502 (2009).

[3] X. Gonze, J.-M. Beuken, R. Caracas, F. Detraux, M. Fuchs, G.-M. Rignanese, L. Sindic, M. Verstraete, G. Zerah, F. Jollet, M. Torrent, A. Roy, M. Mikami, P. Ghosez, J.-Y. Raty, and D. C. Allan, *Computational Materials Science* **25**, 478 (2002).

- [4] X. Gonze, F. Jollet, F. Abreu Araujo, D. Adams, B. Amadon, T. Applencourt, C. Audouze, J.-M. Beuken, J. Bieder, A. Bokhanchuk, E. Bousquet, F. Bruneval, D. Caliste, M. Côté, F. Dahm, F. Da Pieve, M. Delaveau, M. Di Gennaro, B. Dorado, C. Espejo, G. Geneste, L. Genovese, A. Gerossier, M. Giantomassi, Y. Gillet, D. R. Hamann, L. He, G. Jomard, J. Laflamme Janssen, S. Le Roux, A. Levitt, A. Lherbier, F. Liu, I. Lukačević, A. Martin, C. Martins, M. J. T. Oliveira, S. Poncé, Y. Pouillon, T. Rangel, G.-M. Rignanese, A. H. Romero, B. Rousseau, O. Rubel, A. A. Shukri, M. Stankovski, M. Torrent, M. Van Setten, B. Van Troeye, M. J. Verstraete, D. Waroquiers, J. Wiktor, B. Xu, A. Zhou, and J. Zwanziger, *Computer Physics Communications* **205**, 106 (2016).
- [5] F. Bruneval, N. Vast, and L. Reining, *Phys. Rev. B* **74**, 045102 (2006).
- [6] L. J. P. Ament, M. van Veenendaal, and J. van den Brink, *EPL (Europhysics Letters)* **95**, 27008 (2011).
- [7] M. O. Krause and J. H. Oliver, *Journal of Physical and Chemical Reference Data* **8**, 329 (1979), <https://doi.org/10.1063/1.555595>.
- [8] K. Zakeri, T. Engelhardt, T. Wolf, and M. Le Tacon, *Phys. Rev. B* **96**, 094531 (2017).